Sex estimation of the humerus: A geometric morphometric analysis in an adult sample

S. López-Lázaro[a,b,*], A. Pérez-Fernández[c], I. Alemán[c], J. Viciano[d]

[a] Departamento de Antropología, Facultad de Ciencias Sociales, Universidad de Chile, Av. Ignacio Carrera Pinto 1045, 685033 Santiago, Chile
[b] Forensic Dentistry Lab, Centro de Investigación en Odontología Legal y Forense -CIO-, Facultad de Odontología, Universidad de La Frontera, Temuco, Chile
[c] Laboratory of Anthropology, Department of Legal Medicine, Toxicology and Physical Anthropology, School of Medicine, University of Granada, Granada, Spain
[d] Operative Unit of Anthropology, Department of Medicine and Ageing Sciences, 'G. d'Annunzio' University of Chieti–Pescara, Chieti, Italy

A B S T R A C T

Sex estimation is the keystone for positive identification when an unidentified human body is recovered in forensic contexts. However, in complex death scenes such as mass disasters, the remains are often fleshed, mutilated, burned, and/or commingled. In situations such as these where it is not possible to analyze pelvis and/or cranium data, traditional metric and qualitative morphological methods on postcranial bones can yield unsatisfactory results. In such cases, geometric morphometric techniques offer an alternative to the analysis of both shape and size components of morphological variation that can be of great utility for sex estimation in forensic investigations. The study population consisted of 72 well-preserved adult humeri (40 males and 32 females; mean age of 62 years) that were photographed in standardized positions with landmarks located in four two-dimensional views of the humerus (anterior surface of the proximal epiphysis, and anterior, posterior and inferior surface of distal epiphysis). Principal components analysis, canonical variates analysis and discriminant analysis were applied. The data indicated that males and females were classified with low levels of accuracy (54.95–77.92% for males; 56.87–71.78% for females) based on shape variables. However, when the shape variable was combined with the centroid size, the levels of accuracy increased (81.86–94.92% for males; 84.08–94.88% for females). To obtain larger differences between males and females, it is necessary the combination of centroid size with shape variables; the shape of the humerus is insufficient to discriminate sex with accuracy.

1. Introduction

Sex estimation is the keystone of establishing a biological profile of a human skeleton during physical and forensic anthropological analyses. The pelvis is considered the most accurate bone for sex estimation [1–3]. The sexual dimorphism of the pelvis results from selective constraints on males and females forced by locomotion and childbearing [1] and is non-specific to populations, unlike other regions of the skeleton [3,4]. However, postmortem damage and taphonomic changes may prevent the collection and ulterior analysis of this anatomical region for sex estimation [5]. In absence of a pelvis, the skull has been traditionally considered the second-best indicator for sex assessment [6–9] despite several studies based on postcranial skeleton evidence to the contrary [10]. Postcranial elements such as the scapula [11], vertebrae [12], ribs [13], carpal bones [14], the internal auditory canal located on the temporal bone [15], and the hyoid bone [16] show statistically significant sexual dimorphism. Nevertheless, excluding the pelvis, long bones are the postcranial elements that have demonstrated the most effective sex assessment discrimination (e.g. [10,17–19]).

Due to its structure and size, the humerus is considered one of the strongest long bones of the skeleton. Even in a fragmented state of preservation, it is possible to recover it in forensic cases [20–22]. Sexual dimorphism of the humerus has been studied intensively in the last decades mainly following metric and qualitative morphological methods. Most of the studies focused on size differences [10,23–28,29] with good results and producing accuracies of correct assessment of sex ranging from 76.8% to 100%. Qualitative morphological differences have also been analyzed, but to a lesser extent (e.g. [31–34]), providing accuracies ranging from 71.8% to 92%. Although metric methods of sex estimation have very high rates of accuracy and are fairly easy to execute, they have certain disadvantages. Generally, they are population-specific based on sexual dimorphism and varying size patterns that

---

exist across populations [24,35]. Therefore, a method that was created for one specific population may not be wholly accurate when applied to a population of different chronological/geographical origin, resulting in skewed or erroneous sex classifications [36]. Metric methods are also limited because they do not consider the shape of the bone [37]. On the other hand, some subjectivity is involved in qualitative morphological methods because it is very difficult to consistently assign a score to a specific feature; therefore, these methods lend themselves to a high probability of intra- and inter-rater error [38]. However, the application of geometric morphometric techniques can solve these difficulties [37,39].

Geometric morphometrics is a technique that allows the quantification of morphological characteristics and the analysis of both shape and size differences in a two- or three-dimensional (2D or 3D) coordinate system [40–42]. It has strong potential in the field of physical anthropology to quantify sexual dimorphism of skeletal elements because it considers the shape of the elements and the locations of the 2D or 3D landmarks relative to each other. This technique has been used to study sexual dimorphism in, for example, the pelvis [43–46], skull [47–49], mandible [39,50], and teeth [51–53]. Some studies, such as Kranioti et al. [21], Vance and Steyn [54], Maass and Friedling [55] and Ammer [56] investigated sexual dimorphism of the humerus using geometric morphometric techniques, yielding forensically acceptable accuracies in classifying the sex of an individual based on the humerus only. However, the scientific community agrees a population-specific study is required for identification purposes in medico-legal death investigations in order to obtain accurate results in sexing skeletal remains for a given population [36,57].

The aim of this work is to predict sex from the humerus for identification purposes in forensic investigations by using geometric morphometric techniques on two-dimensional photographic images.

2. Material and methods

2.1. Sample

The study sample consisted of 72 adult individuals from the Granada Municipal Cemetery of San José (Spain). Antemortem data were obtained from the records of the San José Municipal Cemetery, the Granada Registry Office, and the Granada Institute of Legal Medicine. Sex, age, and cause of death, among others, were included. The skeletal collection is housed in the Laboratory of Anthropology of the University of Granada, Spain. The age of the individuals ranged from 22 to 85 years. The mean age for males was 52.98 ± 12.13 (N = 40) and for females 71.69 ± 15.24 (N = 32). The great majority of births took place during the five decades between 1901 and 1949 (54.2% of the births) and their deaths occurred during the four decades from 1973 to 2002 (62.5% of the deaths). Exclusion criteria that impeded the collection of humeri from these selected individuals were size and morphological alterations, such as healed antemortem trauma, postmortem fractures, and taphonomic changes or pathological conditions, as these conditions may be a factor of bias.

2.2. Sample photography and locating landmarks and semi-landmarks

Images were taken with a digital camera Canon EOS 1000D (Canon Inc., Japan) and a lens Canon 50 mm f1.8 (Canon Inc., Japan). The humerus was placed in the center of the lens to avoid distortion. The scale was positioned parallel to the humerus and at the same distance from the lens. The left humerus was selected for the study; in case of absence or exclusion, the right humerus was photographed and digitally mirrored. Each humerus was positioned in a standardized manner according to the view, and a photograph was taken with the camera lens at a perpendicular angle to the bone surface.

Landmarks were located in four two-dimensional views of the humerus for geometric morphometric analyses (Fig. 1 and Table 1). The

first view corresponded to the anterior surface of the proximal epiphysis, and five landmarks were selected as defined by Kranioti et al. [21]. The second view corresponded to the anterior surface of the distal epiphysis, and eight landmarks were selected (two landmarks defined by Vance and Steyn [54] and six new landmarks defined and used in the current study). For both first and second views, the orientation of the humerus was achieved by letting the humerus balance on the horizontal plane with the anterior surface facing the camera. The third view corresponded to the posterior surface of the distal epiphysis which documents the shape of the olecranon fossa and the trochlear extension. Twelve landmarks were selected (eight landmarks according to the definitions of Vance and Steyn [54] and four new landmarks defined and used in the current study). The orientation of the humerus was achieved by letting the humerus balance on the horizontal plane with the posterior surface facing the camera. The fourth view corresponded to the inferior surface of the distal epiphysis, which documents the angle of the medial epicondyle and the inferior view of the trochlea. The humerus was placed with the anterior surface facing upwards. Eleven landmarks were placed (ten landmarks according to the definitions of Vance and Steyn [54] and one new landmark defined and used in the current study). All landmarks were digitalized using TPSdig2 software [58].

2.3. Intra- and inter-rater error analysis

Intra- and inter-rater error agreement in locating landmarks was performed by re-digitization of 10 randomly selected humeri by the principal observer and of 10 humeri by the secondary observer. During 5 consecutive days, landmarks were located in 10 images of five humeri. The process was repeated twice with two days between them. Coordinates for intra-rater error were taken by the principal observer. Coordinates for inter-rater error were taken by two observers. To increase observation reliability, the average of the two periods was used. The coordinates were located using TPSdig2 [58]. To quantify observation reliability, the intraclass correlation coefficient (ICC) was calculated, which estimates the mean of correlations between all possible pairs of observations. The ICC range (0–1) was classified according to the criteria proposed by Fleiss [59]: below 0.4 represents poor reliability, between 0.4 and 0.75 represents fair to good reliability, and above 0.75 represents excellent reliability. To determine which landmarks were less repeatable and/or concordant, ICC values were calculated separately for each one.

2.4. Geometric morphometrics and statistical analysis

A Generalized Procrustes Analysis was applied to remove position, orientation, and scale effects. Centroid size was used to scale a configuration of landmarks, and the thin-plate spline (TPS) functions were employed to represent the visualization changes between configuration landmarks.

Principal components analysis (PCA) and canonical variable analysis (CVA) were used to analyze landmark coordinates. PCA is an ordination method for simplifying descriptions of variations among individuals and CVA for simplifying descriptions between groups [42]. The PCA and CVA were performed with PCAGen and CVAGen, respectively [60].

The multivariate normal distribution of the data was verified by the Kolmogorov-Smirnov test and the homogeneity of the variance and covariance was verified by the Box's M. Multivariate analysis of variance (MANOVA) was performed, and Wilks' Lambda was used to reflect the number of significant variables. Discriminant analysis was applied, including the shape variables and shape and size variables combined. Besides, differences in centroid size between sex were analyzed through t-test. Centroid size is the most common size estimator used in geometric morphometrics. These analyses were performed using IBM® SPSS® v.22 software.
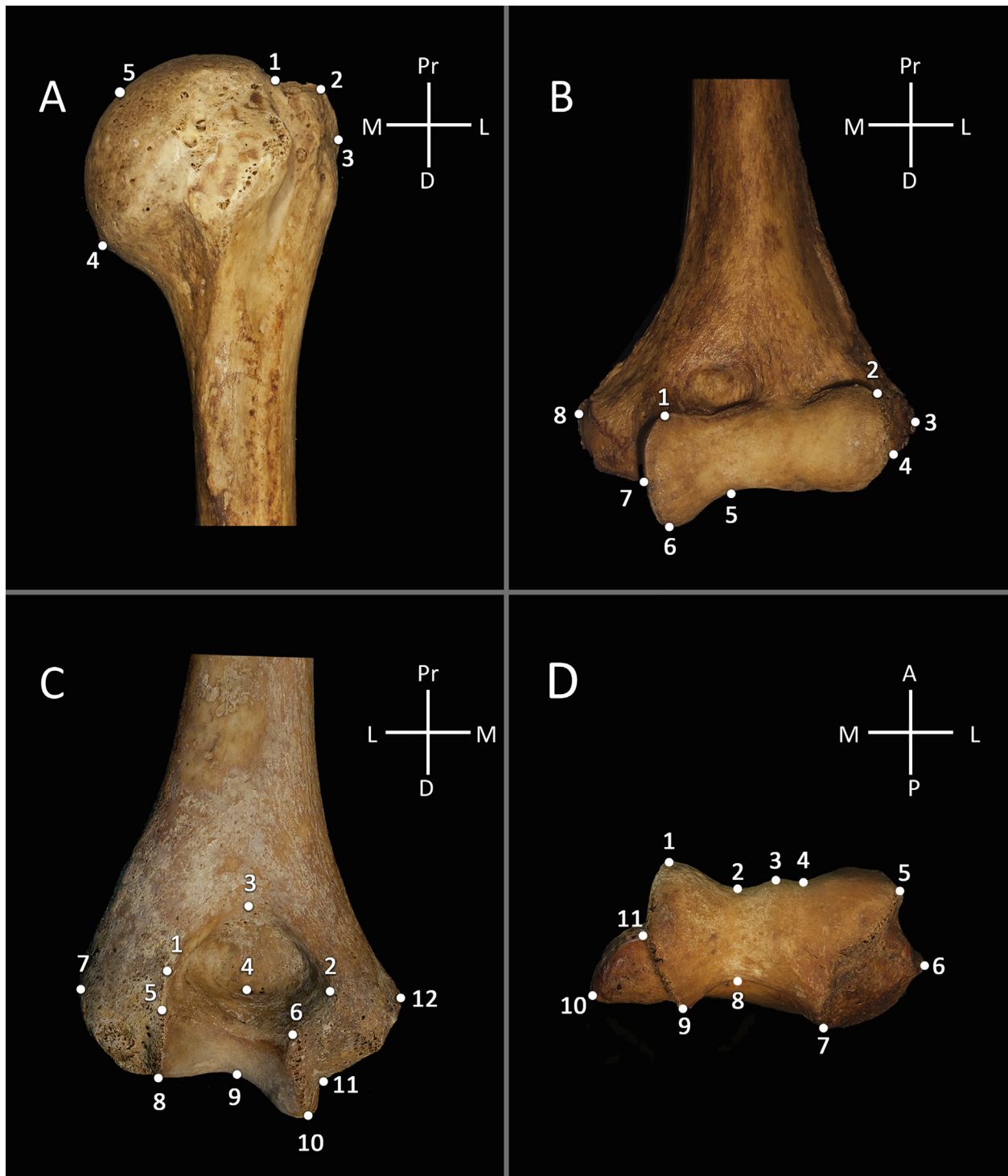
Fig. 1. Location of the defined landmarks points on the humerus in (A) anterior surface of the proximal epiphysis, (B) anterior surface of the distal epiphysis, (C) posterior surface of the distal epiphysis, and (D) inferior surface of the distal epiphysis. Pr, proximal; D, distal; M, medial; L, lateral; A, anterior; P, posterior.

3. Results

3.1. Intra- and inter-rater error analysis

In the intra-rater error analysis (Table 2), the ICC values for the raw coordinates for the four views of the humerus ranged from 0.976 to 1.000, indicating excellent reliability. Regarding the inter-rater error analysis, the ICC values for the raw coordinates ranged from 0.876 to 1.000, indicating excellent reliability. Thus, these ICC values showed

that raw coordinates for landmark locations were concordant and reproducible within and between raters.

3.2. Shape and size analysis of proximal epiphysis

3.2.1. Anterior surface

The PCA included five principal components (PC) that explained 97.94% of the shape variability in the anterior surface of the proximal epiphysis (Table 3). The first two PC of this analysis are plotted in

Table 1
Definition of the landmarks used to represent the shape of humerus on the different views.

Landmark	Definition	References
Anterior surface of the proximal epiphysis		
LM1	The projection of the superior part of the anatomical neck	Kranioti et al. [16]
LM2	The maximum curvature point of the greater tubercle	Kranioti et al. [16]
LM3	The most lateral point of the greater tubercle	Kranioti et al. [16]
LM4	The projection of the medial and inferior part of the head	Kranioti et al. [16]
LM5	The sectioning point on the humeral head outline, of the ortogonal projection of the middle point between landmarks 1 and 4	Kranioti et al. [16]
Anterior surface of the distal epiphysis		
LM1	The superior point of the medial edge of the trochlea	This study
LM2	The superior point of the lateral edge of the capitulum	This study
LM3	The most lateral edge of the lateral epicondyle	Vance and Steyn [16]
LM4	The inferior edge of the capitulum, at the point of the bone where the curved edge becomes a distinct ridge	This study
LM5	The most constricted point of the posterior trochlear "spool"	This study
LM6	The inferior point of the medial edge of trochlea	This study
LM7	The intersection point between the edge of trochlea and the medial epicondyle.	This study
LM8	The most medial point on the medial epicondyle	Vance and Steyn [54]
Posterior surface of the distal epiphysis		
LM1	The most lateral point of the olecranon fossa seen on the posterior surface. This landmark was not placed within the fossa itself, but on the lateral edge of the fossa	Vance and Steyn [54]
LM2	The most medial point of the olecranon fossa seen on the posterior surface. This landmark was not placed within the fossa itself, but on the medial edge of the fossa	Vance and Steyn [54]
LM3	The most superior point of the olecranon fossa	Vance and Steyn [54]
LM4	The inferior edge of the olecranon fossa, in the point of maximum curvature within the fossa itself	This study
LM5	The superior point of the lateral edge of the capitulum	This study
LM6	The superior point of the medial edge of the trochlea	This study
LM7	The most lateral edge of the lateral epicondyle	Vance and Steyn [54]
LM8	The inferior edge of the capitulum, at the point of the bone where the curved edge becomes a distinct ridge	Vance and Steyn [54]
LM9	The most constricted point of the posterior trochlear "spool"	Vance and Steyn [54]
LM10	The inferior edge of the trochlea, at the junction where the straight ridge becomes curved	Vance and Steyn [54]
LM11	The most constricted point in the union between the trochlea and the medial epicondyle	This study
LM12	The most medial point on the medial epicondyle	Vance and Steyn [54]
Inferior surface of the distal epiphysis		
LM1	The superior edge of the trochlea. This landmark was placed where the straight vertical edge of the trochlea becomes curved again	Vance and Steyn [54]
LM2	The most constricted point on the anterior trochlear "spool"	Vance and Steyn [54]
LM3	The most superior point on the anterior trochlear "spool"	This study
LM4	The most constricted point on the anterior capitulum "spool"	Vance and Steyn [54]
LM5	The most lateral margin of the capitulum. This landmark was placed on the point where the curved edge becomes a distinct ridge	Vance and Steyn [54]
LM6	The most lateral point of the lateral epicondyle	Vance and Steyn [54]
LM7	The medial margin of the lateral epicondyle on the inferior ridge of bone that constitutes the posterior surface of the capitulum	Vance and Steyn [54]
LM8	The most constricted point of the trochlear "spool", which constituted the inferior margin of the olecranon fossa	Vance and Steyn [54]
LM9	The most inferior point of the medial margin/ridge of the posterior trochlea	Vance and Steyn [54]
LM10	The most medial point on the medial epicondyle	Vance and Steyn [54]
LM11	The superior "root" of the medial epicondyle, where the superior edge of the medial epicondyle meets the vertical ridge of the trochlea	Vance and Steyn [54]

Fig. 2. PC1 (horizontal axis) accounted for 50.36% of the shape variability while PC2 (vertical axis) explained 20.52% of the variability. Male and female individuals were found to be homogenously distributed along both axes of the PCA dispersion plot. The plot of deformation allowed an easier visualization of the shape variations among landmarks on the PC1 and PC2 axes, illustrating the difference between the consensus shape and the shape change between sexes. Along the x-axis, the positive values of the PC1 described a clear distance between the upper facet of the greater tubercle and its lateral margin, while in the negative values, an approach is observed. PC2 showed a convergence of the midpoint of the humeral head outline and the projection of the superior border of the anatomical neck along the y-axis.

Table 2
Values of ICC for the intra- and inter-rater error analysis for the raw coordinates.

	LM1	LM2	LM3	LM4	LM5	LM6	LM7	LM8	LM9	LM10	LM11	LM12
Anterior surface of the proximal epiphysis												
Intra-rater	0.999	0.987	0.977	0.976	0.998	N/A	N/A	N/A	N/A	N/A	N/A	N/A
Inter-rater	1.000	0.998	0.876	1.000	0.964	N/A	N/A	N/A	N/A	N/A	N/A	N/A
Anterior surface of the distal epiphysis												
Intra-rater	0.999	0.999	1.000	0.999	1.000	1.000	1.000	1.000	N/A	N/A	N/A	N/A
Inter-rater	0.998	0.996	0.999	0.995	1.000	1.000	1.000	1.000	N/A	N/A	N/A	N/A
Posterior surface of the distal epiphysis												
Intra-rater	1.000	1.000	0.999	1.000	0.999	0.999	0.998	1.000	1.000	1.000	1.000	1.000
Inter-rater	0.991	0.973	0.952	0.992	0.962	0.960	0.916	1.000	1.000	1.000	0.995	0.992
Inferior surface of the distal epiphysis												
Intra-rater	0.997	0.995	0.994	0.991	0.993	0.992	0.994	0.995	0.995	0.996	0.996	N/A
Inter-rater	0.996	0.996	0.992	0.994	0.994	0.996	0.996	0.993	0.997	0.995	0.926	N/A

ICC, intraclass correlation coefficient; LM, landmark; N/A, not applicable.

Table 3
Principal components with more of 95% of the total variance explained.

PC	Anterior surface of the proximal epiphysis			Anterior surface of the distal epiphysis			Posterior surface of the distal epiphysis			Inferior surface of the distal epiphysis		
	SV	% EV	% CuV	SV	% EV	% CuV	SV	% EV	% CuV	SV	% EV	% CuV
1	2.33E-03	50.04	52.04	1.89E-03	36.86	36.86	1.32E-03	18.78	18.78	1.40E-03	30.03	30.03
2	8.50E-04	18.96	70.00	9.46E-04	18.50	55.37	8.39E-04	11.97	30.74	6.24E-04	13.36	43.39
3	6.28E-04	13.99	85.00	5.02E-04	9.81	65.18	7.79E-04	11.12	41.86	4.34E-04	9.30	52.69
4	4.11E-04	9.16	94.16	4.58E-04	8.96	74.13	7.10E-04	10.13	51.99	3.96E-04	8.47	61.16
5	1.70E-04	3.80	97.96	3.51E-04	6.87	81.01	5.64E-04	8.05	60.04	3.43E-04	7.34	68.50
6	–	–	–	2.58E-04	5.04	86.04	4.77E-04	6.80	66.85	2.83E-04	6.06	74.55
7	–	–	–	2.27E-04	4.43	90.47	3.86E-04	5.51	72.36	2.36E-04	5.04	79.60
8	–	–	–	1.48E-04	2.89	93.36	3.20E-04	4.57	76.92	2.15E-04	4.60	84.20
9	–	–	–	1.26E-04	2.45	95.82	2.84E-04	4.05	80.97	1.70E-04	3.64	87.84
10	–	–	–	–	–	–	2.39E-04	3.42	84.39	1.20E-04	2.58	90.42
11	–	–	–	–	–	–	1.97E-04	2.81	87.19	1.12E-04	2.39	92.81
12	–	–	–	–	–	–	1.83E-04	2.61	89.80	8.15E-05	1.74	94.56
13	–	–	–	–	–	–	1.46E-04	2.09	91.89	7.23E-05	1.55	96.10
14	–	–	–	–	–	–	1.36E-04	1.93	93.82	–	–	–
15	–	–	–	–	–	–	1.20E-04	1.71	95.53	–	–	–

PC, principal component; SV, Singular value; % EV, percentage of explained variance; % CuV, percentage of cumulative variance.

The scatter plot of the CVA placed the majority of female individuals in the negative values describing a displacement of the maximum curvature point of the greater tubercle towards distal with respect to the projection of the superior border of the anatomical neck (which moved in the opposite direction). Males were allocated along the central and positive values of the canonical variable (Fig. 4).

Discriminant differences (p ≤ 0.05) between variables for both shape and shape + size analyses were shown by Wilks' Lambda test (Table 4). Discriminant analysis according to the leave-one-out cross validation showed a percentage of correct classification of 54.95% and 56.87% in males and females, respectively. However, these values changed to 94.92% [+39.27 pp, an increase of 39.27 percentage points] and 89.55% [+32.68 pp], respectively, after the centroid size variable was added. Significant differences in centroid size were detected between sexes (p ≤ 0.05; Table 5).

3.3. Shape and size analysis of distal epiphysis

3.3.1. Anterior surface

The PCA included nine principal components that explained 95.82% of the shape variability in the anterior surface of the distal epiphysis (Table 3). The first two PC of this analysis are plotted in Fig. 2. PC1 accounted for 36.86% of the shape variability while PC2 explained 18.50% of the variability. Male individuals were homogenously distributed along both axes of the PCA dispersion plot, while females showed a majority concentration in the lower right quadrant of the plot. In comparison with male individuals, female individuals tended to a greater distance between the lateral epicondyle and the lateral edge of the capitulum along the x-axis. Similarly, female individuals showed a greater prominence of the medial epicondyle explained by PC2.

The scatter plot of the CVA placed the majority of male individuals in the center of the plot and in the positive direction, relating their morphology with a displacement of the inferior point of the medial edge of the trochlea towards proximo-lateral direction. The female individuals, located in the center of the plot and in the negative values of the canonical variable, moved in the opposite direction (Fig. 4).

Discriminant differences (p ≤ 0.05) between variables for both shape and shape + size analyses were shown by Wilks' Lambda test (Table 4). Discriminant analysis according to the leave-one-out cross validation showed percentage of correct classification of 63.66% and 63.03% in males and females respectively. However, these values changed (to 86.65% [+22.99 pp; i.e. an increase of 19.12 percentage points] and 84.30% [+21.27 pp], respectively) after the centroid size variable was added. Significant differences in centroid size was detected between sexes (p ≤ 0.05; Table 5).

3.3.2. Posterior surface

The PCA included 15 principal components that explained 95.53% of the shape variability in the posterior surface of the distal epiphysis (Table 3). The first two PC of this analysis are plotted in Fig. 3. PC1 accounted for 18.78% of the shape variability while PC2 explained 11.97% of the variability. Male and female individuals were found to be homogenously distributed along both axes of the PCA dispersion plot. Along the x-axis, the negative values of PC1 described a slight broadening of the epiphysis (i.e. medial and lateral epicondyle moved away from each other), together with a decrease in the longitudinal axis of the superior point of the olecranon fossa; the effect was reversed for the positive values of PC1.

The scatter plot of the CVA showed a clear separation according to sex, with male individuals located in the positive values and females in the negative values (Fig. 4). The shape change between the sexes was explained by the displacement of the inferior edge of the olecranon fossa towards proximo-lateral direction for males, and towards disto-medial for females.

Discriminant differences (p ≤ 0.05) between variables for both shape and shape + size analyses were shown by Wilks' Lambda test (Table 4). Discriminant analysis according to the leave-one-out cross validation showed a percentage of correct classification of 77.92% and 71.78% in males and females, respectively. However, these values changed to 90.77% [+12.85 pp] and 94.88% [+23.10 pp], respectively, after the centroid size variable was added. Significant differences in centroid size were detected between sexes (p ≤ 0.05; Table 5).

3.3.3. Inferior surface

The PCA included 13 principal components that explained 96.10% of the shape variability in the inferior surface of the proximal epiphysis (Table 3). The first two PC of this analysis are plotted in Fig. 3. PC1 accounted for 30.03% of the shape variability while PC2 explained 13.36% of the variability. Male individuals were homogeneously distributed throughout both axes of the PCA dispersion plot. Along the x-axis, the positive values of the PC1 for female individuals described the convergence of the medial and lateral epicondyle to the posterior plane. Along the y-axis, PC2 for female individuals showed the displacement of the inferior margin of the olecranon fossa, with its curvature being more marked in the negative values than in the positive ones.

The scatter plot of the CVA showed a tendency to locate female individuals in the positive values and male individuals in the negative ones (Fig. 4). The most obvious shape change was located in the medial region and was explained by a broader and more rounded superior edge (U-shape type) of the trochlea for the male individuals and a more acute (V-shape type) for the females.
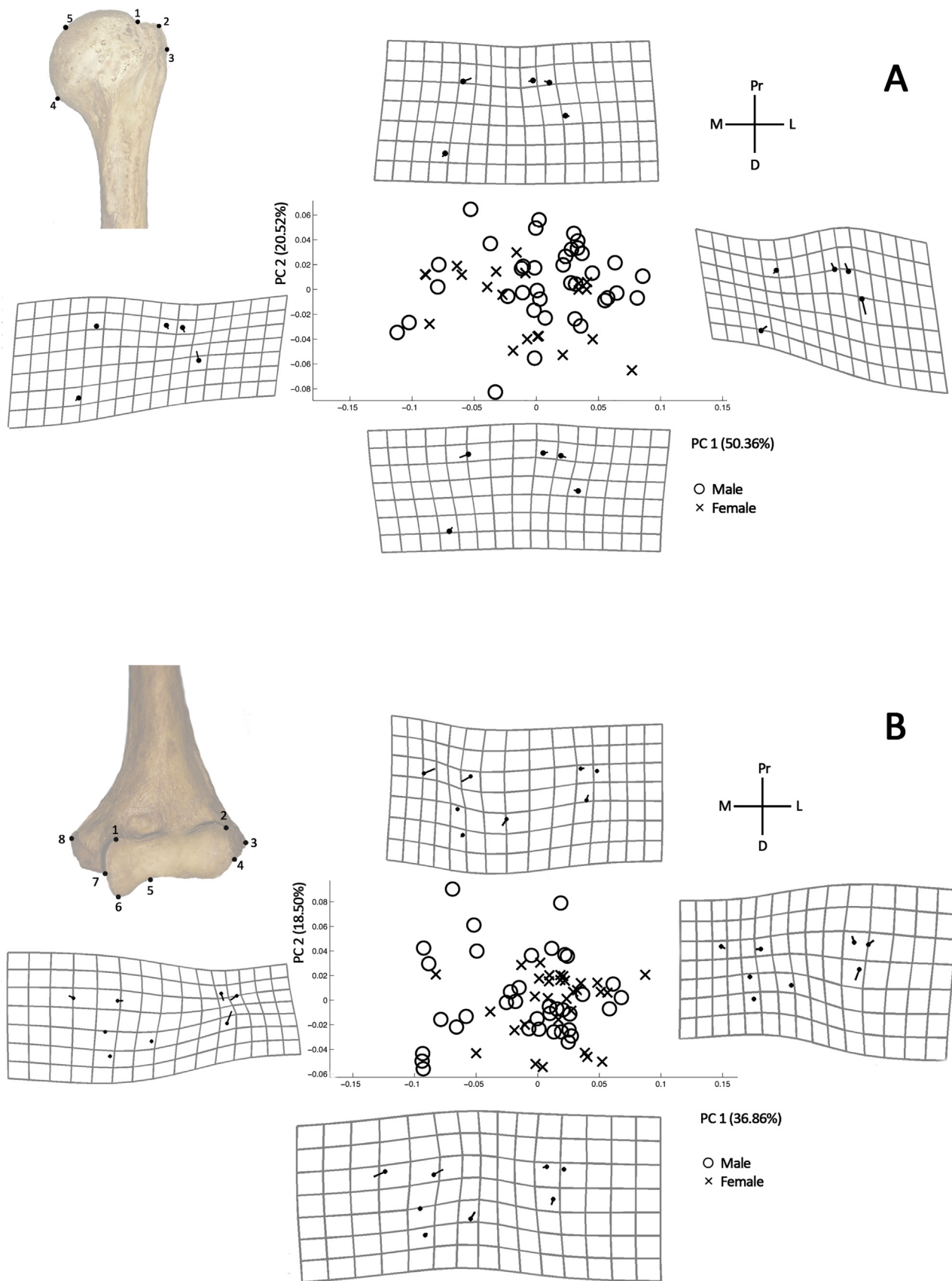
Fig. 2. Principal component analysis scatterplot obtained for the (A) anterior surface of the proximal epiphysis, (B) anterior surface of the distal epiphysis. Thin-plate spline deformations grids and landmark displacement vectors showing shape variation along principal component 1 (PC1) and principal component 2 (PC2) in positive and negative directions. Pr, proximal; D, distal; M, medial; L, lateral; A, anterior; P, posterior.
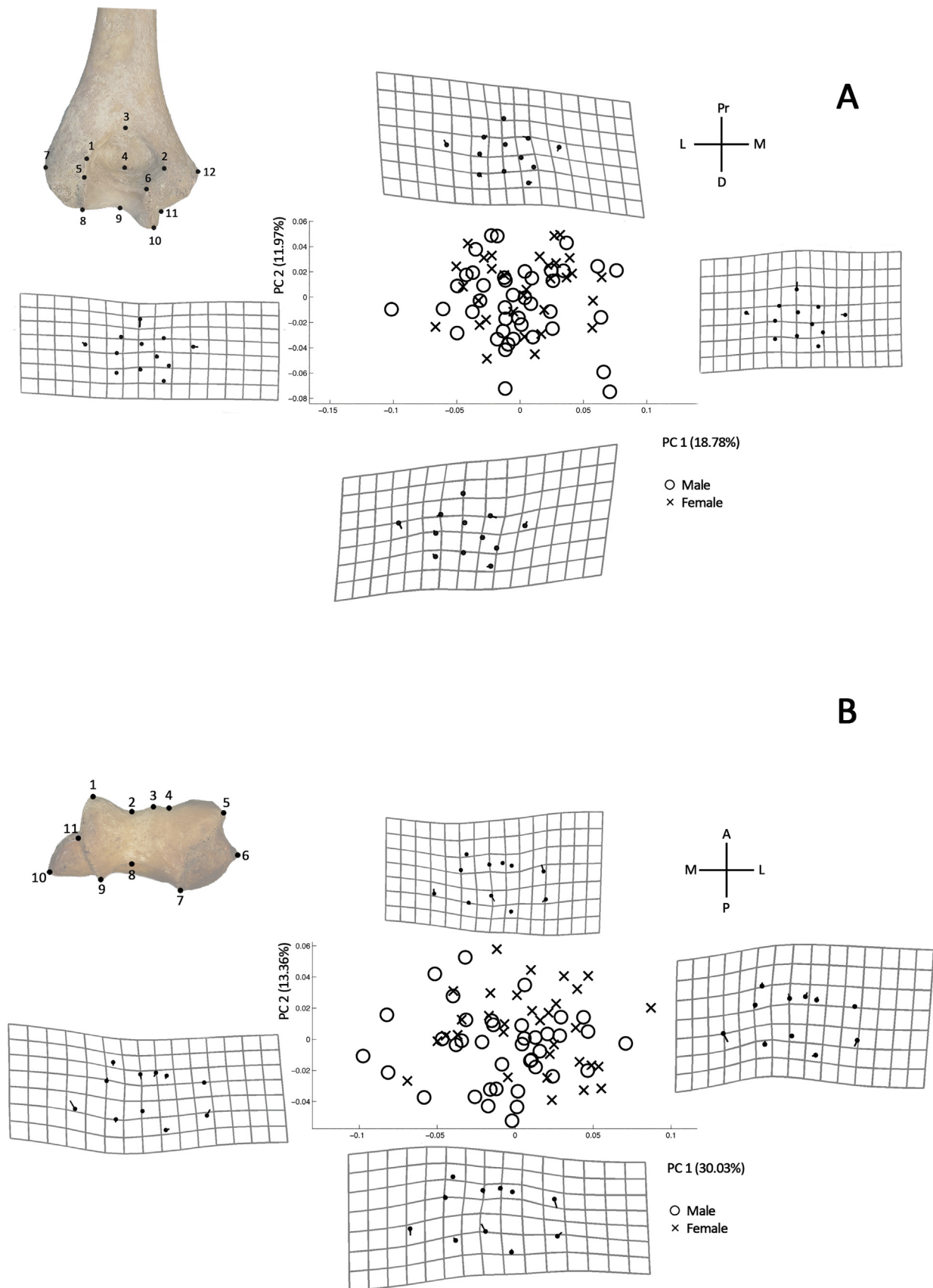
Fig. 3. Principal component analysis scatterplot obtained for the (A) posterior surface of the distal epiphysis, and (B) inferior surface of the distal epiphysis of the humerus shape variables. Thin-plate spline deformations grids and landmark displacement vectors showing shape variation along principal component 1 (PC1) and principal component 2 (PC2) in positive and negative directions. Pr, proximal; D, distal; M, medial; L, lateral; A, anterior; P, posterior.
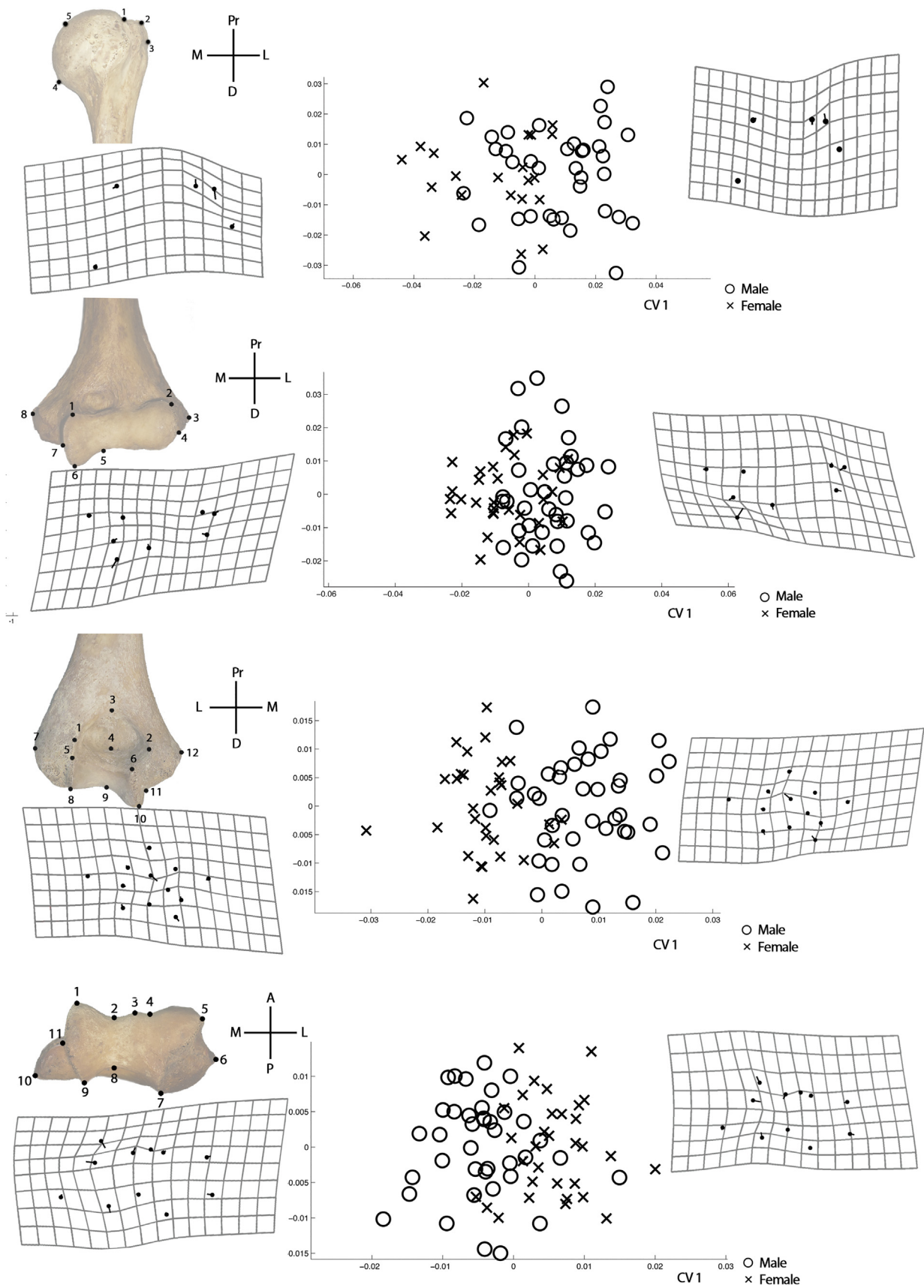
Fig. 4. Canonical variate analysis scatterplot obtained for the (A) anterior surface of the proximal epiphysis, (B) anterior surface of the distal epiphysis, (C) posterior surface of the distal epiphysis, and (D) inferior surface of the distal epiphysis of the humerus shape variables. Thin-plate spline deformations grids and landmark displacement vectors showing shape variation along canonical variate 1 (CV1) in positive and negative directions. Pr, proximal; D, distal; M, medial; L, lateral; A, anterior; P, posterior.

Table 4
Original canonical variable and cross-validation discriminant analysis based on shape and shape + size variables.

| | Lambdás Wilks | | | Classification accuracy by sex | | | | % | |
| | λ | P | | N | Estimated sex | | | | |
					♂	♀		♂	♀
Anterior surface of the proximal humeral epiphysis									
Shape			OR	♂	26	10		65.47	69.03
				♀	8	13			
	0.707	0.006*							
			LOOCV	♂	23	13		54.95	56.87
				♀	11	10			
Shape + size			OR	♂	33	3		95.06	91.95
				♀	1	20			
	0.303	0.000*							
			LOOCV	♂	32	4		94.92	89.55
				♀	1	20			
Anterior surface of the distal humeral epiphysis									
Shape			OR	♂	26	11		70.76	70.48
				♀	9	22			
	0.680	0.026*							
			LOOCV	♂	23	14		63.66	63.03
				♀	11	20			
Shape + size			OR	♂	34	3		87.69	91.48
				♀	4	27			
	0.331	0.000*							
			LOOCV	♂	31	6		86.65	84.30
				♀	4	27			
Posterior surface of the distal humeral epiphysis									
Shape			OR	♂	36	5		90.07	88.10
				♀	3	28			
	0.411	0.000*							
			LOOCV	♂	28	13		77.92	71.78
				♀	6	25			
Shape + size			OR	♂	41	0		96.88	100.00
				♀	1	30			
	0.164	0.000*							
			LOOCV	♂	39	2		90.77	94.88
				♀	3	28			
Inferior surface of the distal humeral epiphysis									
Shape			OR	♂	33	6		84.41	84.58
				♀	5	27			
	0.574	0.015*							
			LOOCV	♂	27	12		68.90	69.08
				♀	10	22			
Shape + size			OR	♂	34	5		100.00	88.89
				♀	0	32			
	0.338	0.000*							
			LOOCV	♂	33	6		81.86	84.08
				♀	6	26			

[a] The percentage indicates the number of individuals correctly classified relative to the total of individuals that presents a particular trait; the classification is weighted by sex.
[b] The percentage indicates the number of individuals correctly classified relative to the total of individuals that presents a particular trait; the classification is weighted with sexes pooled.
N, number of individuals; OR, original variables; LOOCV, leave-one-out cross-validation. The asterisk (*) indicates values statistically significant at $p \leq 0.05$.

Discriminant differences ($p \leq 0.05$) between variables for both shape and shape + size analyses were shown by Wilks' Lambda test (Table 4). Discriminant analysis according to the leave-one-out cross validation showed a percentage of correct classification of 68.90% and 69.08% in males and females, respectively. However, these values changed to 81.86% [+12.96 pp] and 84.08% [+15.00 pp], respectively, after the centroid size variable was added. Significant differences in centroid size were detected between sexes ($p \leq 0.05$; Table 5).

4. Discussion

Several publications provide evidence that sex estimation using long bones has more discriminatory power than the cranium (considered the second-best indicator of sex after the pelvis). Thus, long bones are to be preferred to the cranium for estimating sex when the pelvis is un-available for examination due to the poor state of preservation in burial environments [10,28].

The shape of the humerus is considered a strong morphological indicator of sex because of its relationship to the carrying angle of the arm, which is different in males and females based on morphological differences in their shoulders and hips. While females have wider hips and narrower shoulders, the opposite is true in males [31,61]. In this study, the shape of the humerus showed a statistically significant sexual dimorphism. On the proximal epiphysis, male individuals showed a projected greater tubercle with a pronounced superior border of the anatomical neck than females, who had a smoother greater tubercle with its superior border less pronounced. These results are in agreement with those of Kranioti et al. [21] and Carretero et al. [62], arguing that this configuration may be due to the differences in robusticity between the sexes, with a greater strain on supraspinatus muscle attachment site and articulation surface in males compared to females. On the distal epiphysis, the shape change between the sexes reflected the olecranon fossa shape and the trochlear extension. The more oval/rhomboid shape of the olecranon fossa in females was illustrated in the downward

Table 5
Descriptive statistics for centroid size (in mm) and *t*-test results for mean differences between the sexes.

	Centroid size			*t*-test		
	N	Mean	SD	Mean differences	df	Sig.
Anterior surface of the proximal humeral epiphysis						
Male	37	47.27	2.72	7.95		
				5.31	55	0.000*
Female	21	41.89	1.80			
Anterior surface of the distal humeral epiphysis						
Male	37	65.09	3.61	9.86		
				7.74	66	0.000*
Female	31	57.36	2.69			
Posterior surface of the distal humeral epiphysis						
Male	41	62.73	2.61	12.63		
				7.57	70	0.000*
Female	31	55.16	2.40			
Inferior surface of the distal humeral epiphysis						
Male	39	65.82	5.08	7.88		
				7.74	69	0.000*
Female	32	58.03	2.57			

N, number of individuals; SD, standard deviation; df, degrees of freedom. The asterisk (*) indicates values statistically significant at p ≤ 0.05.

displacement of the inferior edge, acquiring a more triangular shape in males with an upward displacement of the inferior edge of the olecranon fossa. Our results are in agreement with previous studies [31,54,56]. Regarding the trochlear extension, the female trochlea was more asymmetrical, depicted by the extension of the medial trochlea far past its lateral edge; in addition, in inferior view, the superior edge of the trochlea was of a sharper V-shape type. In contrast, males showed a more symmetrical trochlea with a broader and more rounded superior edge (U-shape type). The results obtained in this study about trochlear extension are opposite to those provided by Vance and Steyn [54] using techniques of geometric morphometrics. They found that males showed the inferior margin of the trochlea positioned farther downward (inferiorly) to that of females. The results of Vance and Steyn [54] are in agreement with the qualitative morphologic studies of Rogers [31]. She observed that this trait is asymmetrical in males (with greater extension of the medial trochlea) and more symmetrical in females, and subsequent studies have validated this observation with different populations [30,32–34]. Ammer et al. [56], instead, it does not find differences between sex in the shape of the constriction of the trochlea. The contradiction of our results could be explained by a reverse dimorphism phenomenon. According to Plavcan [63], the term "reverse dimorphism" is used to indicate that females are larger than males. Dimorphism is usually expressed quantitatively (metric data) as a ratio of the larger sex to the smaller; however, in our study using qualitative (morphological) data, we could define reverse dimorphism to indicate that the opposite relation that is most observed in the general population is true. This situation of reverse dimorphism could be influenced by genetic and environmental factors, resulting in large variations in the degree of sexual dimorphism (including reduced dimorphism) across diverse populations. Frayer and Wolpoff [64] attributed the reduction in sexual dimorphism to a "convergence in the requirements of male and female roles". In this way, dimorphic tendencies have increasingly become monomorphic; therefore, sexual variations are continuous variables rather than discrete, an overlap between the sexes is expected, and the reduced sexual dimorphism and consequent male/female overlap has extended to include reverse sexual dimorphism [65]. Given our results, it is necessary to perform additional analyses in this population (with a larger sample) and other populations to confirm the presence of reverse dimorphism in trochlear extension.

Regarding size, in the four two-dimensional views (anterior surface of the proximal epiphysis; and anterior, posterior, and inferior surface of distal epiphysis), the humerus of male individuals had larger mean centroid sizes than those of females. This is in agreement with the results of traditional metric analyses [10,23,25–28] and geometric morphometric studies [21,54–56,61,66] of different population groups. The

larger size of male humeri are likely a reflection of body size dimorphism due to genetic constitution and differential patterns of secondary sexual development, as well as to changes in environmental factors that affect bone growth such as lifestyle, nutrition, and extreme division of labor [64,67,68].

The analyses performed in this study showed that males and females were classified with low levels of accuracy (54.95–77.92% for males; 56.87–71.78% for females) based on shape variables of the proximal and distal humeral epiphysis. However, the levels of accuracy increased when the shape variable was combined with the centroid size (81.86–94.92% for males; 84.08–94.88% for females). These results reflect that the shape of the proximal and distal humeral epiphysis is insufficient to discriminate between sexes, and that the inclusion of size is necessary to obtain larger differences between males and females and, therefore, higher discrimination reliability. Anterior surface of the proximal epiphysis had similar classification rates to the posterior surface of the distal epiphysis (anterior surface of proximal epiphysis: 94.92% for males and 89.55% for females; posterior surface of the distal epiphysis: 90.77% for males and 94.88% for females), while the other views of the distal epiphysis showed lower classification rates (anterior surface of distal epiphysis: 86.65% for males and 84.30% for females; inferior surface of distal epiphysis: 81.86% for males and 84.08% for females). Given these results, it is not possible to conclude which epiphysis is better for sex estimation.

In medico-legal settings, forensic anthropologists must perform theoretical and empirical validation. The established principles and methods may be reliable in certain populations but require an adjustment in others [69]. Variation in sexual dimorphism between populations requires specific standards in forensic contexts [70], and this validation can be also necessary when using historical osteological collections. Several studies have been conducted with identified skeletal collections, since they are recognized as a valuable asset for research [71]. Nevertheless, because of the secular change, the applicability of methods developed in historical samples has been questioned when applied to contemporary populations [72]. In spite of several studies showing the impact of secular trends in forensic anthropology [73–75], the utility of the methods should not be denied [72]. For these reasons, the results of this study require validation using contemporary samples to assure their reliability and validity when applied to current forensic cases.

5. Conclusion

The first and most crucial biological characteristic is to have a correct estimate of sex, as this designation will narrow down by half the number of possible matches in the population. For this purpose, easy and rapid techniques for biological profiling are necessary when fragmentary skeletal remains are recovered in forensic contexts. Using geometric morphometric techniques, differences between humeri of males and females could be observed when proximal and distal epiphysis were analyzed, yielding high levels of classification accuracy.

Declaration of Competing Interest

The authors declare that they have no known competing financial interests or personal relationships that could have appeared to influence the work reported in this paper.

Acknowledgements

References

[1] P. Murail, J. Bruzek, F. Houët, E. Cunha, DSP: A tool for probabilistic sex diagnosis using worldwide variability in hip-bone measurements, Bull. Mémoires La Société d'Anthropologie Paris. (2005) 167–176.

[2] T.W. Phenice, A newly developed visual method of sexing the os pubis, Am. J. Phys. Anthropol. 30 (1969) 297–301, https://doi.org/10.1002/ajpa.1330300214.

[3] J. Buikstra, D. Ubelaker, Standards for data collection from human skeletal remains: proceedings of a seminar at the Field Museum of, Natural History. (1994).

[4] M. Steyn, M.L. Patriquin, Osteometric sex determination from the pelvis—Does population specificity matter? 113.e1-113.e5, Forensic Sci. Int. 191 (2009), https://doi.org/10.1016/J.FORSCIINT.2009.07.009.

[5] T.R. Peckmann, K. Orr, S. Meek, S.K. Manolis, Sex determination from the calcaneus in a 20th century Greek population using discriminant function analysis, Sci. Justice. 55 (2015) 377–382, https://doi.org/10.1016/J.SCIJUS.2015.04.009.

[6] M.Y. İşcan, Forensic anthropology of sex and body size, Forensic Sci. Int. 147 (2005) 107–112, https://doi.org/10.1016/J.FORSCIINT.2004.09.069.

[7] R.J. Muckle, Introducing Archaeology, University of Toronto Press, Ontario, 2014.

[8] W. Bass, Human osteology: a laboratory and field manual, 5th ed., Missouri Archaeological Society, Columbia, 2005.

[9] R. Pickering, D. Bachman, The use of forensic anthropology, CRC Press, 2009.

[10] M.K. Spradley, R.L. Jantz, Sex estimation in forensic anthropology: skull versus postcranial elements, J. Forensic Sci. 56 (2011) 289–296, https://doi.org/10.1111/j.1556-4029.2010.01635.x.

[11] A.E. Koukiasa, C. Eliopoulos, S.K. Manolis, Biometric sex estimation using the scapula and clavicle in a modern Greek population, Anthropol. Anzeiger. 74 (2017) 241–246, https://doi.org/10.1127/anthranz/2017/0658.

[12] A. Amores, M.C. Botella, I. Alemán, Sexual Dimorphism in the 7th Cervical and 12th Thoracic Vertebrae from a Mediterranean Population, J. Forensic Sci. 59 (2014) 301–305, https://doi.org/10.1111/1556-4029.12320.

[13] A.M. Kubicka, J. Piontek, Sex estimation from measurements of the first rib in a contemporary Polish population, Int. J. Legal Med. 130 (2016) 265–272, https://doi.org/10.1007/s00414-015-1247-6.

[14] P. Mastrangelo, S. De Luca, I. Alemán, M.C. Botella, Sex assessment from the carpals bones: Discriminant function analysis in a 20th century Spanish sample, Forensic Sci. Int. 216 (e1–216) (206 2011), e10, , https://doi.org/10.1016/j.forsciint.2011.01.007.

[15] D. Gonçalves, T.J.U. Thompson, E. Cunha, Sexual dimorphism of the lateral angle of the internal auditory canal and its potential for sex estimation of burned human skeletal remains, Int. J. Legal Med. 129 (2015) 1183–1186, https://doi.org/10.1007/s00414-015-1154-x.

[16] R. D'Anastasio, J. Viciano, M. Di Nicola, D.T. Cesana, M. Sciubba, M. Del Cimmuto, A. Paolucci, A. Fazio, L. Capasso, Estimation of sex from the hyoid body in skeletal individuals from archeological sites, Homo. 65 (2014) 311–321, https://doi.org/10.1016/j.jchb.2014.01.002.

[17] E. González-Reimers, J. Velasco-Vázquez, M. Arnay-de-la-Rosa, F. Santolaria-Fernández, Sex determination by discriminant function analysis of the right tibia in the prehispanic population of the Canary Islands, Forensic Sci. Int. 108 (2000) 165–172, https://doi.org/10.1016/S0379-0738(99)00205-4.

[18] G.C. Krüger, E.N. L'Abbé, K.E. Stull, Sex estimation from the long bones of modern South Africans, Int. J. Legal Med. 131 (2017) 275–285, https://doi.org/10.1007/s00414-016-1488-z.

[19] R. Purkait, Triangle identified at the proximal end of femur: a new sex determinant, Forensic Sci. Int. 147 (2005) 135–139, https://doi.org/10.1016/j.forsciint.2004.08.005.

[20] T. Waldron, The relative survival of the human skeleton: implications for paleopathology, in: J.R.A. Boddington, A.N. Garland (Eds.), Death, Decay Reconstr, Manchester University Press, Manchester, 1987, pp. 55–64.

[21] E.F. Kranioti, M. Bastir, A Sánchez-Meseguer, A Rosas, A geometric-morphometric study of the cretan humerus for sex identification, Forensic Sci. Int. 189 (2009) 111.e1–111.e8, https://doi.org/10.1016/j.forsciint.2009.04.013.

[22] A. Galloway, P. Willey, L. Snyder, Human bone mineral densities and survival of bone elements: a contemporary sample, in: M.H. Sorg, W.D. Haglund (Eds.), Forensic Taphon, CRC Press, Boca Raton, Postmortem Fate Hum. Remain., 1997, pp. 295–317.

[23] M. Steyn, M.Y. İşcan, Osteometric variation in the humerus: sexual dimorphism in South Africans, Forensic Sci. Int. 106 (1999) 77–85, https://doi.org/10.1016/S0379-0738(99)00141-3.

[24] J. Albanese, H.F.V. Cardoso, S.R. Saunders, Universal methodology for developing univariate sample-specific sex determination methods: an example using the epicondylar breadth of the humerus, J. Archaeol. Sci. 32 (2005) 143–152, https://doi.org/10.1016/J.JAS.2004.08.003.

[25] L.R. Frutos, Metric determination of sex from the humerus in a Guatemalan forensic sample, Forensic Sci. Int. 147 (2005) 153–157, https://doi.org/10.1016/j.forsciint.2004.09.077.

[26] E.F. Kranioti, M. Michalodimitrakis, Sexual dimorphism of the humerus in contemporary cretans - A population-specific study and a review of the literature, J. Forensic Sci. 54 (2009) 996–1000, https://doi.org/10.1111/j.1556-4029.2009.01103.x.

[27] M.S. Robinson, M.A. Bidmos, The skull and humerus in the determination of sex: Reliability of discriminant function equations, Forensic Sci. Int. 186 (2009) 86.e1–86.e5, https://doi.org/10.1016/j.forsciint.2009.01.003.

[28] D. Charisi, C. Eliopoulos, V. Vanna, C.G. Koilias, S.K. Manolis, Sexual Dimorphism of the Arm Bones in a Modern Greek Population, J. Forensic Sci. 56 (2011) 10–18, https://doi.org/10.1111/j.1556-4029.2010.01538.x.

[29] M.L. Tise, M.K. Spradley, B.E. Anderson, Postcranial Sex Estimation of Individuals Considered Hispanic, J. Forensic Sci. 58 (2013) S9–S14, https://doi.org/10.1111/1556-4029.12006.

[30] T. Rogers, Sex determination of adolescent skeletons using the distal humerus, Am. J. Phys. Anthropol. 140 (2009) 143–148, https://doi.org/10.1002/ajpa.21060.

[31] T. Rogers, A visual method of determining the sex of skeletal remains using the distal humerus, J. Forensic Sci. 44 (1999) 57–60, https://doi.org/10.1520/JFS14411J.

[32] V. Wanek, A., Qualitative Analysis for Sex Determination in Humans Utilizing Posterior and Medial Aspects of the Distal Humerus, Portland State University, 2000.

[33] V.L. Vance, M. Steyn, E.N. L'Abbé, Nonmetric sex determination from the distal and posterior humerus in black and white South Africans, J. Forensic Sci. 56 (2011) 710–714, https://doi.org/10.1111/j.1556-4029.2011.01724.x.

[34] C.G. Falys, H. Schutkowski, D.A. Weston, The distal humerus–a blind test of Rogers' sexing technique using a documented skeletal collection, J. Forensic Sci. 50 (2005) 1289–1293, https://doi.org/10.1520/JFS2005171.

[35] G.A. Macho, Is sexual dimorphism in the femur a "population specific phenomenon"? Z. Morphol. Anthropol. 78 (1990) 229–242.

[36] W.M. Krogman, M.Y. Iscan, The human skeleton in forensic medicine, CC Thomas, Springfield, Illinois, 1986.

[37] P. Gonzalez, V. Bernal, S. Perez, Analysis of sexual dimorphism of craniofacial traits using geometric morphometric techniques, Int. J. Osteoarchaeol. 21 (2009) 82–91, https://doi.org/10.1002/oa.1109.

[38] B.A. Williams, T.L. Rogers, Evaluating the Accuracy and Precision of Cranial Morphological Traits for Sex Determination, J. Forensic Sci. 51 (2006) 729–735, https://doi.org/10.1111/j.1556-4029.2006.00177.x.

[39] D. Franklin, C.E. Oxnard, P. O'Higgins, I. Dadour, Sexual dimorphism in the subadult mandible: Quantification using geometric morphometrics, J. Forensic Sci. 52 (2007) 6–10, https://doi.org/10.1111/j.1556-4029.2006.00311.x.

[40] F.L. Bookstein, Morphometric tools for landmark data: geometry and biology, Cambridge University Press, Cambridge, 1991.

[41] D.E. Slice, Modern morphometrics in physical anthropology, Springer, Nueva York, 2005.

[42] M.L. Zelditch, D.L. Swiderski, H. Sheets, Geometric Morphometrics for Biologists: A Primer, Academic Press, London, 2012.

[43] P.N. González, V. Bernal, S. Ivan Perez, Analysis of dimorphic structures of the human pelvis: its implications for sex estimation in samples without reference collections, J. Archaeol. Sci. 34 (2007) 1720–1730, https://doi.org/10.1016/j.jas.2006.12.013.

[44] J.A. Bytheway, A.H. Ross, A Geometric Morphometric Approach to Sex Determination of the Human Adult Os Coxa, J. Forensic Sci. 55 (2010) 859–864, https://doi.org/10.1111/j.1556-4029.2010.01374.x.

[45] E.J. Estévez, S. López-Lázaro, C. López-Morago, I. Alemán, M.C. Botella, Sex estimation of infants through geometric morphometric analysis of the ilium, Int. J. Legal Med. 131 (2017) 1747–1756, https://doi.org/10.1007/s00414-017-1659-6.

[46] E.J. Estévez Campo, S. López-Lázaro, C. López-Morago Rodríguez, I. Alemán Aguilera, M.C. Botella López, Specific-age group sex estimation of infants through geometric morphometrics analysis of pubis and ischium, Forensic Sci. Int. 286 (2018) 185–192, https://doi.org/10.1016/j.forsciint.2018.03.012.

[47] E.H. Kimmerle, A. Ross, D. Slice, Sexual Dimorphism in America: Geometric Morphometric Analysis of the Craniofacial Region, J. Forensic Sci. 53 (2008) 54–57, https://doi.org/10.1111/j.1556-4029.2007.00627.x.

[48] H. Green, D. Curnoe, Sexual dimorphism in Southeast Asian crania: A geometric morphometric approach, HOMO. 60 (2009) 517–534, https://doi.org/10.1016/j.jchb.2009.09.001.

[49] M.-E. Chovalopoulou, E.D. Valakos, S.K. Manolis, Sex determination by three-dimensional geometric morphometrics of the vault and midsagittal curve of the neurocranium in a modern Greek population sample, Homo. 67 (2016) 173–187, https://doi.org/10.1016/j.jchb.2015.09.007.

[50] A.C. Oettlé, E. Pretorius, M. Steyn, Geometric morphometric analysis of the use of mandibular gonial eversion in sex determination, HOMO. 60 (2009) 29–43, https://doi.org/10.1016/j.jchb.2007.01.003.

[51] G. Polychronis, P. Christou, M. Mavragani, D.J. Halazonetis, Geometric morphometric 3D shape analysis and covariation of human mandibular and maxillary first molars, Am. J. Phys. Anthropol. 152 (2013) 186–196, https://doi.org/10.1002/ajpa.22340.

[52] S. López-Lázaro, I. Alemán, J. Viciano, J. Irurita, M.C. Botella, Sexual dimorphism of the first deciduous molar: A geometric morphometric approach, Forensic Sci. Int. 290 (2018) 94–102, https://doi.org/10.1016/j.forsciint.2018.06.036.

[53] R. Yong, S. Ranjitkar, D. Lekkas, D. Halazonetis, A. Evans, A. Brook, G. Townsend, Three-dimensional (3D) geometric morphometric analysis of human premolars to assess sexual dimorphism and biological ancestry in Australian populations, Am. J. Phys. Anthropol. 166 (2018) 373–385, https://doi.org/10.1002/ajpa.23438.

[54] V.L. Vance, M. Steyn, Geometric morphometric assessment of sexually dimorphic characteristics of the distal humerus, HOMO- J. Comp. Hum. Biol. 64 (2013) 329–340, https://doi.org/10.1016/j.jchb.2013.04.003.

[55] P. Maass, L.J. Friedling, Morphometric analysis of the humerus in an adult South African cadaveric sample, 451.e1-451.e9, Forensic Sci. Int. 289 (2018), https://doi.org/10.1016/J.FORSCIINT.2018.04.037.

[56] S. Ammer, J. d'Oliveira Coelho, E.M. Cunha, Outline shape analysis on the trochlear constriction and olecranon fossa of the humerus: insights for sex estimation and a new computational tool, J. Forensic Sci. 64 (2019) 1788–1795, https://doi.org/10.1111/1556-4029.14096.

[57] D. Franklin, L. Freedman, N. Milne, C.E. Oxnard, A geometric morphometric study of sexual dimorphism in the crania of indigenous southern Africans, S. Afr. J. Sci. 102 (2006) 229–238.

[58] F.J. Rohlf, The tps series of software, Hystrix, Ital. J. Mammal. 26 (2015) 9–12, https://doi.org/10.4404/hystrix-26.1-11264.

[59] J.L. Fleiss, Design and analysis of clinical experiments, John Wiley & Sons, Nueva York, 1986.

[60] H.D. Sheets, IMP-Integrated Morhpmetrics packge, (2011). http://www3.canisius.edu/~sheets/.

[61] H. Tanaka, P.E. Lestrel, T. Uetake, S. Kato, F. Ohtsuki, Sex differences in proximal humeral outline shape: elliptical Fourier functions, J. Forensic Sci. 45 (2000) 292–302, https://doi.org/10.1002/ajpa.10011.

[62] J.M. Carretero, C. Lorenzo, J.L. Arsuaga, Análisis multivariante del húmero en la colección de restos identificados de la Universidad de Coimbra (Portugal), Antropol. Port. 13 (1995) 139–156.

[63] J.M. Plavcan, Sexual dimorphism in primate evolution, Am. J. Phys. Anthropol. Suppl 33 (2001) 25–53, https://doi.org/10.1002/ajpa.10011.

[64] D.W. Frayer, M.H. Wolpoff, Sexual dimorphism, Annu. Rev. Anthropol. 14 (1985) 429–473, https://doi.org/10.1146/annurev.an.14.100185.002241.

[65] J. Viciano, R. D'Anastasio, L. Capasso, Odontometric sex estimation on three populations of the Iron Age from Abruzzo region (central–southern Italy), Arch. Oral Biol. 60 (2015) 100–115, https://doi.org/10.1016/j.archoralbio.2014.09.003.

[66] E.F. Kranioti, D. Nathena, M. Michalodimitrakis, Sex estimation of the Cretan humerus: A digital radiometric study, Int. J. Legal Med. 125 (2011) 659–667, https://doi.org/10.1007/s00414-010-0470-4.

[67] L. Scheuer, S. Black, C. Cunningham, Developmental Juvenile Osteology, Academic Press, London, 2000.

[68] M.E. Hamilton, Sexual dimorphism in skeletal samples, in: R.L. Hall (Ed.), Sex. Dimorphism Homo Sapiens — A Quest. Size, Praeger Publishers, New York, 1996, pp. 107–163.

[69] A.M. Christensen, C.M. Crowder, Evidentiary Standards for Forensic Anthropology, J. Forensic Sci. 54 (2009) 1211–1216, https://doi.org/10.1111/j.1556-4029.2009.01176.x.

[70] M.Y. Işcan, Progress in forensic anthropology: the 20th century, Forensic Sci. Int. 98 (1998) 1–8, https://doi.org/10.1016/s0379-0738(98)00133-9.

[71] C. Sanabria-Medina, G. González-Colmenares, H.O. Restrepo, J.M.G. Rodríguez, A contemporary Colombian skeletal reference collection: A resource for the development of population specific standards, 577.e1-577.e4, Forensic Sci. Int. 266 (2016), https://doi.org/10.1016/J.FORSCIINT.2016.06.020.

[72] A.R. Klales, Secular change in morphological pelvic traits used for sex estimation, J. Forensic Sci. 61 (2016) 295–301, https://doi.org/10.1111/1556-4029.13008.

[73] P. Guyomarc'h, J. Velemínská, P. Sedlak, M. Dobisíková, I. Švenkrtová, J. Brůžek, Impact of secular trends on sex assessment evaluated through femoral dimensions of the Czech population, 284.e1-284.e6, Forensic Sci. Int. 262 (2016), https://doi.org/10.1016/J.FORSCIINT.2016.02.042.

[74] D.C. Martin, M.E. Danforth, An analysis of secular change in the human mandible over the last century, Am. J. Hum. Biol. 21 (2009) 704–706, https://doi.org/10.1002/ajhb.20866.

[75] L. Manthey, R.L. Jantz, M. Bohnert, K. Jellinghaus, Secular change of sexually dimorphic cranial variables in Euro-Americans and Germans, Int. J. Legal Med. 131 (2017) 1113–1118, https://doi.org/10.1007/s00414-016-1469-2.